The Cryosphere Discuss., 5, 1123–1166, 2011
www.the-cryosphere-discuss.net/5/1123/2011/
doi:10.5194/tcd-5-1123-2011

The Cryosphere Discussions

Deriving mass balance and calving variations from reanalysis data and sparse observations, Glaciar San Rafael, northern Patagonia, 1950–2005

M. Koppes[1], H. Conway[2], L. A. Rasmussen[2], and M. Chernos[1]

[1]Dept. of Geography, University of British Columbia, Vancouver, BC V6T 1Z2, Canada
[2]Dept. Earth & Space Sciences, University of Washington, Seattle, WA 98195, USA

Received: 29 March 2011 – Accepted: 3 April 2011 – Published: 14 April 2011

Correspondence to: M. Koppes (koppes@geog.ubc.ca)

Published by Copernicus Publications on behalf of the European Geosciences Union.

Abstract

Mass balance variations of Glaciar San Rafael, the most equatorial tidewater glacier in the North Patagonian Icefield, are reconstructed over the period 1950–2005 using NCEP-NCAR reanalysis climate data together with sparse, local historical observations of air temperature, precipitation, accumulation, ablation, thinning, calving, and glacier retreat. The combined observations over the past 50 yr indicate that Glaciar San Rafael has thinned and retreated since 1959, with a total mass loss of ~22 km^3 of ice equivalent. Over that period, except for a short period of cooling from 1998–2003, the climate has become progressively warmer and drier, which has resulted primarily in pervasive thinning of the glacier surface and a decrease in calving rates, with only minor acceleration in retreat of the terminus. A comparison of calving fluxes derived from the mass balance variations and from theoretical calving and sliding laws suggest that calving rates are inversely correlated with retreat rates, and that terminus geometry is more important than changes in balance fluxes to the terminus in driving calving dynamics. For Glaciar San Rafael, regional climate warming has not yet resulted in the significant changes in glacier length seen in other calving glaciers in the region, emphasizing the complex dynamics between climate inputs, topographic constraints and glacier response in calving glacier systems.

1 Introduction

Recent observations from Patagonia indicate widespread thinning and retreat of the outlet glaciers that drain the Icefields (Rignot et al., 2003; Rivera et al., 2007), some of the last remaining large reserves of ice outside of the polar ice sheets. This retreat is likely caused in part by regional warming of ~0.5 °C over the past 40 yr (Rasmussen et al., 2007). Many of these outlet glaciers terminate in fjords or lakes, and their response to climate is complicated by their sensitivity to non-climatic influences such as terminus geometry, sediment delivery to the terminus, ice-front melt rates, and water depth

TCD
5, 1123–1166, 2011

(Meier and Post, 1987; Powell, 1991; van der Veen, 1996; Warren and Aniya, 1999; Motyka et al., 2003; O'Neel et al., 2005; Pfeffer, 2007; Rignot et al., 2010). Hence, retreat histories of such tidewater glaciers contain a record both of past climate and of changing ice-front dynamics.

Results from numerical models of the response of the Patagonian Icefields over glacial to interglacial timescales show that (1) glacier mass balance is sensitive to changes in large-scale atmospheric circulation, and (2) estimates of mass balance of tidewater glaciers are highly sensitive to the parameterizations used to model calving (Hulton et al., 1994; Hubbard, 1997; Cook et al., 2003). Today, as during much of the Quaternary, strong westerly winds and the orographic influence of the north-south trending Andes result in high precipitation on the western side of the Andes and relatively low precipitation on the lee side. Conditions during the early Holocene were more arid and may have been up to 6 °C cooler because westerlies were weaker (Mayr et al., 2007), and ocean currents in the region were cooler (Lamy et al., 2004). To better understand how these cooler, more arid conditions may have affected the mass balance of the icefields, a closer look at the response of these outlet glaciers to recent climatic changes is needed.

Here we use a glacier mass balance model and NCEP-NCAR reanalysis data (Kalnay et al., 1996; Kistler et al., 2001), constrained by sparse observations of local climate and glacier change to reconstruct the surface mass balance variations of Glaciar San Rafael, the only tidewater glacier that drains the Northern Patagonian Icefield. The icefield, also known as the Hielo Patagonico Norte (HPN – Fig. 1) extends from approx. 46.5° to 47.5° S, covering an area of ~4200 km^2, and the highest peak, Monte San Valentin, rises to 3910 m. Of the 41 glaciers draining the HPN, 20 of them end in freshwater lakes or fjords. San Rafael is the only glacier that calves into seawater; it is also the most equatorial tidewater glacier in the world. Our primary goal in reconstructing the mass balance history of Glaciar San Rafael is to document ongoing glacier and climate changes in Patagonia, one of the largest and most sensitive remaining areas of temperate ice and a potentially significant contributor to sea level

TCD
5, 1123–1166, 2011

rise (Rignot et al., 2003). Our secondary goal is to demonstrate how sparse glacier observations can be used to constrain a glacier mass balance history, based on global climate models, for regions where the local and regional climate history is not well documented. A further goal is to compare our observation-driven model results to a suite of calving "laws" to help interpret the dominant drivers of tidewater calving.

2 Regional climate history

The HPN is located in the "roaring Forties", a region characterized by a cool, wet climate throughout the year, with frequent precipitation-bearing storms. Ice cover in the region is sustained by this extreme precipitation; Escobar et al. (1992) estimated present-day annual precipitation of 6.7 m water equivalent averaged over the HPN. Seasonal variations in precipitation and temperature are small; summers are wet and windy (Fujiyoshi et al., 1987) and precipitation can fall as snow year-round (Kondo and Yamada, 1988). Although seasonal variations are small, interannual variations in precipitation can be large (Enomoto and Nakajima, 1985); Warren and Sugden (1993) suggested that these large interannual variations in precipitation exert a strong control on glacier dynamics. They also noted that decadal mean temperature and precipitation are positively correlated; when the climate is warmer, it is also wetter.

Reconstructing local climate 1950–2005

The NCEP-NCAR Reanalysis climate database is derived from historical observations of various meteorological variables made at the surface, from radiosondes and from satellites (Kalnay et al., 1996; Kistler et al., 2001). The database consists of estimates of meteorological variables at geopotential heights throughout the troposphere on a 1.9° global grid extending back to January 1948. The nearest NCEP-NCAR gridpoint to Glaciar San Rafael, at 46.67° S, 75° W, is shown as a star in Fig. 1 and henceforth referred to as SR1. Rasmussen et al. (2007) used the NCEP-NCAR data to show

TCD
5, 1123–1166, 2011

that the 850-hPa precipitation flux at 45° S (calculated from $U_{850}RH_{850}$ where U_{850} is the component of the wind from direction 270° and RH_{850} is the relative humidity) decreased by about 10% over 1948–1998. However, the fraction falling as snow at 850 hPa (calculated from $U_{850}RH_{850}$ when $T \leq 2\,^{\circ}C$) decreased by about 20%; hence, the combined effects of warming and drying have caused the 850-hPa snowfall at 45° S to decrease by about 28%.

Although we show model results from 1950 to 2005 using the NCEP-NCAR dataset, caution is needed when interpreting results from 1950 to 1960 because of the inhomogeneity in the instrumental record in the late 1950s (see Rasmussen et al., 2007). For this reason, herein we focus our analysis on climate and glacier changes from 1960 to 2005.

We compared NCEP-NCAR derived climate data from SR1 with temperature and precipitation measurements that we made between March 2005 and April 2006 at a Chilean Forest Service (CONAF) guard station, located about 7 km from the glacier front on the shores of Laguna San Rafael (LSR, at 46.66° S, 73.86° W). We used two tipping bucket rain gauges (0.2 mm per tip) and a 2-channel temperature sensor. Air temperature (measured 1.4 m above the surface) and soil temperature (measured 2 cm below the surface) were recorded hourly. Figure 2 shows daily-average temperature and precipitation measurements at LSR, and NCEP-NCAR derived values at the 1000-hPa level at SR1. A linear regression of temperatures over the period of record yields:

$$T_{LSR} = 0.73\,T_{SR1} + 5.5 \quad (r^2 = 0.77;\ n = 398;\ p < 0.0001) \tag{1}$$

where T_{LSR} is the daily-average air temperature (°C) at Laguna San Rafael, and T_{SR1} is the daily-average 2-m air temperature at SR1.

The correlation between the temperatures measured at LSR and NCEP-NCAR derived surface temperatures at SR1 (Eq. 1) show a good fit, with temperatures at Laguna San Rafael on average 5 °C warmer than at SR1 (Fig. 2a). In contrast, the precipitation-correlation over the same period is weak, accounting for less than half the variance (Fig. 2b); although the NCEP-NCAR values capture the timing of storm events well,

TCD
5, 1123–1166, 2011

the magnitude of the larger storms is generally underestimated. The correlation is improved by including the zonal wind speed U_{SR1} ($m\,s^{-1}$) modeled at 10 m above ground to reflect the magnitude of storm intensity:

$$P_{LSR} = 0.78\,P_{SR1} + 0.91|U_{SR1}| + 0.82 \quad (r^2 = 0.50;\ n = 398;\ p < 0.0001) \tag{2}$$

where P_{LSR} and P_{SR1} are daily precipitation in mm at Laguna San Rafael and the NCEP-NCAR gridpoint SR1, respectively. We note that wind speeds measured near the terminus of San Rafael in 1983 were ~4–5 $m\,s^{-1}$ (Kobayashi and Saito, 1985), while NCEP-NCAR derived winds at SR1 are typically 2–3 times stronger (10–15 $m\,s^{-1}$) for the same period.

We use Eq. (1) and the NCEP-NCAR database to estimate daily-average temperatures at the terminus of Glaciar San Rafael from 1950 to 2005. We also use the NCEP-NCAR upper air temperatures from 1000, 925, 850, 700, and 600 hPa levels to reconstruct daily variations in the atmospheric lapse rate at SR1. The average lapse rate over the period of record was $5.5 \pm 0.9\,°C\,km^{-1}$: the wet lapse rate (where $P_{SR1} > 0$) averaged $5.6\,°C\,km^{-1}$, and the dry lapse rate averaged $4.8\,°C\,km^{-1}$. We used the daily temperature at LSR (calculated using Eq. 1) and the daily lapse rates to reconstruct $T(z)$ from sea level to the top of the glacier. Daily $T(z)$ profiles are needed to partition the snow-fraction of precipitation (Sect. 4.1) and to estimate ablation (Sect. 3.5) over the glacier surface.

Figure 3a shows variations of mean annual temperature variations at Laguna San Rafael over the period 1950–2005, derived from the NCEP-NCAR record. Mean annual temperatures at the glacier front varied only 1.3° C about a mean of 8.9° C, consistent with the strong maritime influence on the climate of the region.

We use Eq. (2) to estimate daily precipitation at Laguna San Rafael over the same period 1950–2005. Annual precipitation there has varied by ±0.60 m about a mean of 3.60 m (Fig. 3b). Precipitation, which was relatively high during the period 1950–1975, decreased by more than 13% during the period 1976 to 2005.

TCD
5, 1123–1166, 2011

To estimate daily precipitation in the form of snowfall over the surface of the glacier $P(z)$ over the period 1950–2005, we scaled P_{LSR} by an orographic enhancement factor $k(z)$ that varies spatially, so that:

$$P(z) = k(z)P_{LSR} \quad (3)$$

The enhancement factor $k(z)$ is not well constrained; sparse observations and model results suggest that precipitation on the plateau of the Northern Patagonian Icefield, ~10 km upwind of the Andean crest, is 2.5 to 5 times that on the outer coast to the west of Laguna San Rafael (Fujiyoshi et al., 1987; Escobar et al., 1992; Carrasco et al., 2002); observations from the Southern Alps of New Zealand, a similar north-south trending mountain belt protruding into the Southern Westerlies, also indicate that precipitation increases to a peak 20 km upwind of the divide that is 4–5 times that on the western coast (Wratt et al., 2000). To test the sensitivity of the enhancement factor $k(z)$, we ran our accumulation model using a range of values from $k = 3$ to $k = 5$ (see Sect. 4.1). We also ran a scenario wherein we assume $k(z)$ varies with distance from the coast (x) and with altitude according to a simplified 1-D orographic model, in which model parameters include the meteoric fall rate, moisture scale height, moist static stability for upward advection, and horizontal wind speed (Smith and Barstad, 2004; Roe, 2005). Whereas the factor k varies as a function of (z), it is also possible to calculate it as a function of distance from the coast and rangefront (x), because the elevation of the glacier surface itself is a function of that distance (see Fig. 4). We tuned the model so that the average precipitation at the coast (~1.8 m a^{-1}) (Carrasco et al., 2002) increases by a factor of two to match observations at Laguna San Rafael (~3.6 m a^{-1}), ~20 km inland, and by a factor of 3.5 at 1200 m a.s.l. to match values estimated by Fujiyoshi et al. (1987) and Carrasco et al. (2002) near the equilibrium line of the glacier. Figure 5 shows modeled spatial variations of $k(z)$.

TCD
5, 1123–1166, 2011

3 Glacier observations

Glaciar San Rafael descends steeply from the HPN through several icefalls, and calves into Laguna San Rafael, a brackish lagoon that is connected with the ocean. A prominent arcuate moraine bounds the western side of the lagoon, while the eastern margin is an abrupt escarpment formed by the Liquine-Ofqui megafault. San Rafael is one of few tidewater glaciers in the Southern Hemisphere that has been periodically, if sparsely, monitored over the past few decades. Aniya (1988, 1999), Warren (1993), Warren et al. (2005) and Rivera et al. (2007) documented both the retreat of the ice front over the past century and recent thinning. While the termini of many of the calving glaciers draining the western edge of the HPN have, until the most recent decade, remained near their Little Ice Age maxima, Glaciar San Rafael has steadily retreated more than 8 km since the end of the Little Ice Age, approx. 1900 AD (Araneda et al., 2007; Koppes et al., 2010).

3.1 Surface geometry and topography

We used data from the Shuttle Radar Topography Mission in 2000 (SRTM-2000) to construct a digital elevation model (DEM) of Glaciar San Rafael (Fig. 4). We also mapped the bathymetry of Laguna San Rafael using ship-board sonar in 2005 and 2006 (Koppes, 2007; Koppes et al., 2010) (Fig. 6) to construct the submarine terminus cross-sectional area. Analysis of the glacier DEM, which has horizontal resolution of ~50 m, indicates that the present-day area of the glacier is 728 km^2 (Fig. 4); it drains ~19% of the HPN icefield. Almost 40% of the surface area of the glacier lies within the "ELA zone", between ~1075–1460 m, as modeled from the Reanalysis data (see Sect. 3.5). Figure 5 shows the current area-altitude distribution of the glacier. The ELA zone also corresponds to the peak in orographic precipitation $k(z)$; this is discussed further in Sect. 4.1.

TCD
5, 1123–1166, 2011

3.2 Surface velocity

Surface velocities of up to 8 km a^{-1} have been observed near the terminus of Glaciar San Rafael, using velocity stakes measured over the month of December (summer) and extrapolated to annual velocities (Naruse, 1985; Kondo and Yamada, 1988; Warren et al., 1995; Willis et al., 2010), making it one of the fastest flowing glaciers worldwide. Rignot et al. (1996) used synthetic aperture radar interferometry (InSAR) and feature tracking methods to measure the longitudinal surface velocity profile in 1994. Measurements from 1994 show centerline velocities that decreased from 4–6 km a^{-1} near the terminus, to 1.3 km a^{-1} 6 km upglacier from the terminus, to 1.1 km a^{-1} near the equilibrium line (~1100 m a.s.l., 17 km upglacier from the terminus). Additional InSAR measurements from Radarsat images taken in 2001 show surface velocities near the terminus decreased to 2.8–3 km a^{-1} (E. Rignot, personal communication, 2003). We note that these velocities were measured by tracking features at the glacier surface, and hence include both longitudinal strain rates and crevasse opening rates; true terminus velocities could be smaller, and the ice flux delivered to the terminus calculated using these velocities would be correspondingly smaller; hence, these ice velocities represent an upper bound for modeling calving rates.

3.3 Calving

Glaciar San Rafael is an actively calving glacier; calving events from both above and below the waterline occur every few minutes. Warren et al. (1995) observed calving events during the summers of 1993 and 1994 and estimated that the mean summer calving flux was $\sim 2 \times 10^{-3}$ km^3/day, with an annual flux of 0.73 km^3 a^{-1}, assuming that calving rates do not vary appreciably across the seasons. The validity of this assumption is supported by our observations of calving events during midwinter 2005 and again in autumn 2006, which indicate similar calving fluxes of 0.75 km^3 a^{-1}. Both estimates are slightly less than estimates from InSAR-derived velocities in 2001 and ASTER-derived velocities from 2007 near the terminus: terminus velocities of

TCD
5, 1123–1166, 2011

2.8 km a^{-1} in 2001 (E. Rignot, personal communication, 2003), and up to 6 km a^{-1} (Willis et al., 2010) during a two-week period in 2007, combined with a terminus ice front area of 0.42 km^2 for 2001–2007 deriveed from the lagoon bathymetry, imply that the calving flux in 2001 was ~1.2 km^3 a^{-1}, and in 2007 was up to ~2.6 km^3 a^{-1} (M. Willis, personal communication, 2010).

3.4 Retreat history

Glaciar San Rafael has been in stop-start retreat throughout the 20th century. Since 1978, the glacier has retreated into a narrowing valley that crosses the Andean range front, and the terminus has changed from an extensive piedmont lobe approx. 7 km wide, to a narrow ~2 km calving front. Figure 6 shows a compilation of terminus positions that we derived from: (1) aerial photos taken by the Chilean and US Air Forces in 1945 and 1959; (2) Landsat and ASTER images collected since 1979; (3) field observations, including a series of paint marks on the northern fjord wall that marked the yearly position of the northern edge of the calving cliff from 1983 to 2002; (4) measurements using ship-borne radar in 2005 and 2006; and (5) observations collated by Warren (1993). Anecdotal evidence from the Chilean Park Service, as well as these observations, suggest that although Glaciar San Rafael has undergone short-term, seasonal advances of the terminus, it has not experienced a multi-year re-advance at any time during the past 50 yr. Given the evidence, we assume that the terminus was either stable or retreating between years in which the terminus position was mapped, and we interpolate the rate of retreat between the known locations of the terminus over time using a cubic spline (Fig. 7).

Prominent trimlines along the valley walls provide a history of ice thickness change during this period. Rivera et al. (2007) compared Landsat MSS and ETM+ images from 1975 and 2001 and estimated an average thinning of the icefield surface of 1.8 ± 1.0 m a^{-1} around the margins of the HPN, while the terminus positions of most of the outlet glaciers were either stable or in slow retreat. Similar rates of thinning

TCD
5, 1123–1166, 2011

($1–2\,m\,a^{-1}$) over the ablation zone of San Rafael were estimated by Aniya (1999) between 1981 and 1998 using photogrammetric methods, and by Willis et al. (2010; $\sim 2.3\,m\,a^{-1}$) between 2001–2007 using repeat ASTER satellite imagery. In July 2005, we measured a prominent trimline 120 m directly above the terminus ice cliff using a laser rangefinder. An early photo taken by the Chilean Air Force shows that the glacier surface was at this trimline in 1945; thinning in the vicinity of the present-day terminus has therefore averaged $\sim 2\,m\,a^{-1}$ since 1945.

In 2005–2006, the glacier terminated in an ice cliff 2-km wide (see Fig. 6). We used a laser rangefinder to determine that the top of the ice cliff varied from 30 to 70 m above water line. Our bathymetric measurements indicate that the glacier terminates in water up to 256 m deep near the centerline, with water depths decreasing to ~140 m on either side of a narrow central trough; the 2005 area of the terminus A_{term} above and below the waterline is $0.42\,km^2$ (Fig. 7). We estimate the annual history of the terminus area A_{term} from 1950 to 2005 using the interpolated terminus locations and our new high resolution map of the bathymetry of Laguna San Rafael (Fig. 6), assuming that the average ice cliff height above water line did not change appreciably during this time. Results in Fig. 7 show a marked change in terminus area (and retreat rate) when the calving front retreated into the narrowing valley in the early 1980s.

3.5 Ablation

Measurements by Ohata et al. (1985a, b) from a network of 17 stakes set along a transect extending from near the terminus of Glaciar San Rafael up to 1050 m a.s.l. indicated that the average rate of ablation near the terminus during December 1983 was $6.8\,cm\,day^{-1}$ in ice equivalent, with daily-average ice ablation decreasing with elevation at a rate of $6\,cm\,km^{-1}$. We use concurrent temperature measurements made at Laguna San Rafael by Enomoto and Nakajima (1985), together with temperature profiles $T(z)$ from NCEP-NCAR data (Sect. 2), to establish a relationship between daily-average ablation $m(z)$ and temperature $T(z)$, considering only $T(z) > 0\,^{\circ}C$:

TCD
5, 1123–1166, 2011

$$(z) = 0.66\,T(z) \quad \text{[ice]} \quad (r^2 = 0.40, n = 49, p < 0.0001) \tag{4a}$$

where $\dot{a}(z)$ is in cm day^{-1} ice equivalent. It should be noted that the ablation stakes used to derive Eq. (4a) were all drilled in ice (Ohata et al., 1985). To estimate ablation of snow, we follow results from Braithwaite and Oleson (1989) and assume that the positive degree-day factor for snow is 3/8th that for ice. That is, for snow:

$$\dot{a}(z) = 0.25\,T(z) \quad \text{[snow]} \tag{4b}$$

In our mass balance model (Sect. 4), we track whether precipitation on the previous day fell as rain or as snow at each elevation z, and then choose either Eq. (4a) or (4b) to estimate daily ablation at z accordingly.

3.6 Surface mass balance and equilibrium line altitudes

The few point measurements of net mass balance that have been collected near San Rafael glacier range from −24.8 m ice eq. at the terminus (Ohata et al., 1985a), +3.5 m water eq. at an elevation of 1296 m a.s.l. on the icefield plateau during 1985 (Yamada, 1987), to +2.2 m water eq. at an elevation of 1500 m a.s.l. on Glacier Nef on the lee (east) side of the icefield during 1997 (Matsuoka and Naruse, 1999). Although sparse, these observations provide useful constraints for tuning both $k(z)$ to estimate the accumulation profile (Eq. 3), and the two ablation co-efficients (Eq. 4a and 4b). Equilibrium line altitude (ELA) observations from prior studies range from: 1250 m a.s.l. in 1984 (Aniya, 1988), 1100 m a.s.l. in 1994 (Rignot et al., 1996) and 1100 m a.s.l. in 2002 (Rivera et al., 2007). These provide additional impotant constraints for our mass balance model (see Sect. 4).

TCD
5, 1123–1166, 2011

4 Glacier mass budget model

4.1 Surface mass balance model

At each elevation z, the annual surface mass balance $\dot{b}(z)$ is the algebraic sum of accumulation $\dot{c}(z)$ and ablation $\dot{a}(z)$. That is:

$$\dot{b}(z) = \dot{c}(z) - \dot{a}(z) \quad (5)$$

We derive daily accumulation and ablation for each elevation z over the glacier surface and sum the totals to calculate the net surface mass balance. Following previous work we assume that any precipitation $P(z)$ that falls when $T(z) > +2\,^{\circ}\mathrm{C}$ is rain that runs off the glacier surface without refreezing. Conversely, when $T(z) \leq +2\,^{\circ}\mathrm{C}$, precipitation falls as snow and accumulates on the glacier surface (Rasmussen and Conway, 2001; Roe, 2005). We calculate accumulation over the entire glacier surface daily, using Eqs. (2) and (3) and temperature to discriminate between rain and snow, and sum the daily accumulation to calculate the annual accumulation at each elevation (z). Model results for the mean annual net mass balance profiles (Fig. 8) and the equilibrium line altitude of Glaciar San Rafael for the period 1950–2005 (Fig. 9) show that the annual ELA (i.e., where $b(z) = 0$) ranges from 1050–1460 m a.s.l.

The concentration of orographic enhancement $k(z)$ of snowfall near the ELA (~1100–1400 m a.s.l.), as indicated by observations (Fujiyoshi et al., 1987; Escobar et al., 1992; Carrasco et al., 2002) may also be a major driver in our mass balance model. An orographically-induced peak in precipitation at the ELA would tip the balance towards net accumulation if too large, or net ablation if too small. As the area-elevation distribution of this glacier is so heavily weighted in a zone across the broad plateau of the icefield at the elevation of the ELA that accounts for almost 40% of the glacier surface, any estimates of the net balance over the past 50 yr are extremely sensitive to the spatial and temporal distribution of an orographically-enhanced peak in precipitation in this zone.

TCD
5, 1123–1166, 2011

4.2 Terminus mass budget

The fundamental equation describing fluxes near the terminus of calving glaciers is:

$$\frac{dL}{dt} = \frac{Q_{\text{bal}} + Q_{\text{thin}} - Q_{\text{calv}}}{A_{\text{term}}} \tag{6}$$

where $\frac{dL}{dt}$ is any change in the length of the glacier; Q_{bal} is the surface mass balance $b(z)$ integrated over the area of the glacier, and Q_{thin} is the volume of ice lost due to thinning. The flux of ice away from the terminus Q_{calv} includes both calving and mass loss due to melting averaged over the area of the terminus face A_{term}. A glacier is in balance when Q_{calv} equals Q_{bal}, and the ice thickness and length are not changing. For a shrinking glacier, the ice volume decreases both through glacier shortening $Q_{\text{term}} = -\frac{dL}{dt} A_{\text{term}}$ and through surface lowering $Q_{\text{thin}} = -\frac{dh}{dt} A_{\text{thin}}$. Glacier retreat $\frac{dL}{dt}$ can be measured from known terminus positions and A_{term} can be estimated from bathymetry, glacier thinning $\frac{dh}{dt}$ and the area of thinning A_{thin} can be estimated from trimlines, and surface mass balance Q_{bal} can be estimated from precipitation and temperature data, and so we rearrange Eq. (6) to solve explicitly for the calving flux Q_{calv}, which is a measure of the volume of ice passing through the terminus per unit time:

$$Q_{\text{calv}} = Q_{\text{bal}} + Q_{\text{thin}} + Q_{\text{term}} \tag{7}$$

Variability in the calving flux, averaged over the terminus cross-sectional area A_{term}, represents temporal changes in the cross-sectionally averaged ice velocity, which primarily arise from changes in sliding speeds for fast moving glaciers like San Rafael.

4.3 Calving model

A second means of deriving the calving flux, Q_{calv}, can be acquired by applying a suite of empirically and theoretically derived "calving laws" (Benn et al., 2007) to a known fjord bathymetry, where former locations of the calving margin are also known. In such a model, the calving rate is quantified by combining the retreat rate $\frac{dL}{dt}$ over time with

TCD
5, 1123–1166, 2011

modeled terminus velocities U_{ice}, and then compared to ice front cross-sectional areas A_{term} to compute a calving flux at annual time steps. The calving rate, U_D, is defined as the difference between the modeled average downslope terminus velocity and the change in terminus position in the L-direction over time; the modeled change in calving flux Q_{calv}, is U_D averaged over the terminus cross-sectional area A_{term} for each time step.

5 Results

5.1 Surface mass balance

The various degree-day models (Eq. 4a and 4b) and precipitation models (Eq. 3) were run to calculate annual ablation Q_{abl}, accumulation Q_{acc} and surface mass balance $Q_{bal} = Q_{acc} - Q_{abl}$ in ice eq. over the glacier for the period 1960 to 2005 (Fig. 11). On the assumption that the uncertainties for each of the model inputs are uncorrelated, the errors for each element were propagated as a sum of squares, with uncertainty up to one standard derivation for the variables used in Eqs. (3) and (4). The results of the various model runs, and the corresponding sensitivities in the range of inputs used, are also summarized in Table 1.

Figure 11a shows annual accumulation and ablation calculated over the glacier surface. Average ablation over the period 1960 to 2005 is 4.2 $km^3\,a^{-1}$. Anomalously low ablation from 1999 to 2003 was a result of anomalously low annual temperatures during that period (see Fig. 3a). Although accumulation (snowfall) depends on the joint distribution of precipitation and temperature, the pattern of accumulation varies most closely with that of precipitation (see Fig. 3b); accumulation was relatively high during the period 1960–1975 and decreased by more than 14% during the period 1976 to 2005.

Scaling the precipitation at Laguna San Rafael, as given in Eq. (3) by a constant $k = 3$ over the area of the glacier (Table 1, case 1, 2), implies the average Q_{acc} today is ~4.0 $km^3\,a^{-1}$; using constant $k = 5$ (Table 1, case 3) implies Q_{acc} is ~6.7 $km^3\,a^{-1}$;

TCD
5, 1123–1166, 2011

using $k(z)$ (Table 1, case 4) implies Q_{acc} is ~5.1 $km^3 a^{-1}$ (Fig. 11a). The range of accumulation values from the various model runs and indicated by the thin black lines, and the range of ablation values by the grey lines. The best fit between observations and modeled surface mass balance and annual ELA occurs when using $k(z)$ and both snow and ice degree-day models (case 4) (see Figs. 8 and 9); we henceforth used the results of that model run to compare Q_{bal} to the other fluxes in the terminus mass budget (see Fig. 12).

Figure 11b shows the range of annual surface mass balance Q_{bal} over the period 1950 to 2005 from case 4 (see Table 1). Surface mass balance was positive in the 1960s, negative in the late 1970s–early 1980s and again in the late 1980s, and was relatively positive from 1999 to 2003, mainly due to reduced ablation during the latter period (Fig. 11a). Average net surface mass balance over the period 1960 to 2005, using $k(z)$ and both snow and ice degree-day models (case 4), was +1.06 $m a^{-1}$. In other words, if the glacier had terminated on land and did not calve, other things being equal we would expect it would still be expanding to capture more surface ablation area in order to reach equilibrium with the present-day climate.

5.2 Length changes

An important non-climatic control on any length changes of a calving glacier is the area of the ice front in contact with fjord water and subject to submarine melt, as documented at Le Conte Glacier (Motyka et al., 2003) and more recently in west Greenland (Rignot et al., 2010). Any decrease in the cross-sectional area of the submarine ice front would diminish the volume of ice subject to melting and calving and hence decrease terminus retreat, assuming the flux of ice to the terminus does not vary significantly. Figure 7 shows that the rate of retreat of the terminus of San Rafael Glacier decreased as the cross-sectional area (A_{term}) in contact with the warm brackish waters of the lagoon diminished in the early 1980s and again in the early 1990s, once the ice front retreated into the steadily narrowing but deepening outlet across the Andean range front.

TCD
5, 1123–1166, 2011

The volume of ice lost from the glacier snout due to retreat during this period (Q_{term}) and its variability over time can be calculated from the subsurface fjord bathymetry (Fig. 6), the height of the above board glacier surface, and the retreat rate (Fig. 7). The terminus has retreated 4 km during the period 1959–2005, with no documented re-advances over this time. If we assume an average ice cliff height of 40 m above a constant lake level has persisted since 1959, the volume of ice lost from the terminus during retreat averaged 0.06 $km^3\,a^{-1}$ over 1959–2005, with a maximum loss of up to 0.17 $km^3\,a^{-1}$ during a phase of rapid retreat in the early 1980s. A second phase of rapid retreat occurred around 1990, with losses of up to 0.12 $km^3\,a^{-1}$. These two periods of rapid retreat followed years when the balance flux (Q_{bal}) was most negative, and hence less ice was arriving at the terminus. Both periods of rapid retreat ended when the terminus retreated into the narrowing outlet valley. Most notably, the mass loss from the terminus during years of rapid retreat was less than 32% of the surface mass deficit; in other words, although the glacier retreated rapidly during those years, at least 2/3 of the mass loss was due to thinning of the glacier itself.

5.3 Thinning flux

If we use thinning rates estimated from satellite images and photos (Aniya, 1999; Rivera et al., 2007; Willis et al., 2010), and from trimlines near the terminus which averaged 2–2.3 m a^{-1} near the current terminus and approached 1–2 m a^{-1} across the lower reaches of the icefield plateau, the total volume of ice lost via thinning at the glacier surface Q_{thin} during 1950–2005 approaches 19 km^3, resulting in an average annual volume loss of 0.35 $km^3\,a^{-1}$. San Rafael glacier hence appears to have lost mass through surface lowering ~6 times, on average, the rate it lost mass through retreat of the calving front. In other words, and similar to observations from neighboring glaciers of the North Patagonian Icefield (Rivera et al., 2007), Glaciar San Rafael appears to be responding to the warmer and drier climate of the past 50 yr by thinning much more strongly than by accelerated calving and frontal retreat.

TCD
5, 1123–1166, 2011

Much of this thinning is most likely due to ice motion in the ablation zone drawing down the glacier surface. Thinning can also result from accelerated surface mass loss due to ablation rates exceeding accumulation. Thinning rates have likely varied significantly over the past 50 yr, and may have been particularly high during the last two decades of the 20th century (when they were last measured in detail), particularly in the period 1978–1989 when ablation fluxes exceeded accumulation fluxes by on average $0.55\,km^3\,a^{-1}$ and by up to $1.2\,km^3\,a^{-1}$ ice eq. in the lower reaches of the glacier. If we assume that the calving flux must always be positive (i.e., $Q_{calv} > 0$ in Eq. (7), no ice accretion at the terminus), Q_{thin} must have been enhanced by excess surface melt of up to $0.9\,km^3\,a^{-1}$ during 1978–1989, when Q_{bal} was negative. There is certainly the possibility that there were years in which $Q_{thin} < 0$ when the climate was cooler and wetter, particularly during the period 1950–1970 and again around 1998–2003, although there is no observational evidence to indicate thickening of the glacier during these periods.

Given the potential influence of calving speeds and retreat of the terminus on longitudinal extension in the terminal zone (e.g., Venteris et al., 1997), the rate of dynamic surface lowering in the terminal zone must also have varied significantly during this period, but by how much is unknown, for only two direct measurements of the surface elevation of the lower reach of the glacier exist, in 1975 and 2001 (Rivera et al., 2007). To first order, the rate of dynamic surface lowering at any point on the glacier is a function of the change in glacier length and the local surface slope; that is, thinning rates decrease upglacier from the terminus. Since we have little data to constrain the variability in dynamic thinning rates over the period, and noting that the parabolic longitudinal glacier surface profile is roughly maintained but shifts upvalley during retreat, we can calculate the rate of ice volume decrease represented by surface lowering and infer the temporal variability in the rate of thinning by combining the retreat history and trimlines on the valley walls and either (1) assume that an average thinning rate of $2\,m\,a^{-1}$ was maintained across the glacier surface throughout the period 1950–2005 (to arrive at the average thinning rate of $0.35\,km^3\,a^{-1}$ stated above), or (2) assume that

TCD
5, 1123–1166, 2011

the dynamic thinning rate equals the product of the retreat rate and surface slope of the glacier in the lower reaches of the glacier, and then decreases upglacier to vanishing values at the glacier headwall. Calculated in this latter way, the rate of ice volume lost to dynamic thinning increased to over 1 $km^3\,a^{-1}$ in the early 1980s and again in the late 1980s, when retreat accelerated markedly and calving rates increased. The combined thinning rate from dynamic surface lowering coupled with excess melt in the ablation zone most likely increased to almost 4 $m\,a^{-1}$ in the lower reaches of the glacier during this period.

6 Modeling the calving flux

We modeled the calving flux in two ways. In our first scenario, we used the mass budget model to estimate the flux of ice delivered to and calved from the terminus over time Q_{calv} using Eq. (7) and compared this flux with the retreat rate in Fig. 12. For a calving glacier in steady-state, where $Q_{thin} = 0$ and $Q_{term} = 0$, any $Q_{bal} > 0$ must be lost through the glacier snout via calving (Q_{calv}). Since the volume of San Rafael glacier has decreased through both shortening (retreat, Q_{term}) and surface lowering (thinning, Q_{thin}) over the past 50 yr, the calving flux Q_{calv} also takes into account these ice mass losses ($Q_{bal} + Q_{thin} + Q_{term}$), as given in Eq. (7). Using this approach and our mass budget model, the calving flux during the period 1960 to 2005 averaged 1.2 $km^3\,a^{-1}$ (black line in Fig. 12), which is similar to fluxes calculated using InSAR in 2001. The grey shading in Fig. 12 bounds the cumulative sources of error in the accumulation and ablation fluxes used when calculating Q_{bal} and hence Q_{calv}.

As seen in Fig. 12 and Table 1, Q_{calv} as modeled using the mass budget has also varied significantly during the past half century. For examples, assuming scenario #4 (where precipitation scales with $k(z)$ and degree day models prescribed in Eq. 4a and 4b) the resulting calving flux Q_{calv} averaged 1.9 $km^3\,a^{-1}$ during the period 1960–1975, and decreased to less than 0.4 $km^3\,a^{-1}$ in the 1980s, a decade when surface melt rates increased and snow accumulation decreased so that all new accumulation was lost through ablation and all calving resulted in net volume loss from the glacier. Q_{calv}

TCD
5, 1123–1166, 2011

slowly increased in the 1990s to more than 3 $km^3 a^{-1}$, but then decreased in the first years of the 21st century. The corresponding calving rates range from $<1\,km\,a^{-1}$ to $>7\,km\,a^{-1}$ over the 1960–2005 period, in agreement with observations (Kondo and Yamada, 1985; Rignot et al., 1996; Willis et al., 2010), and averaged 2.2 $km\,a^{-1}$.

In a second, comparative scenario, the calving flux is driven by sliding at the terminus, and we use the observed bathymetry of the fjord to calculate the thickness of the calving front at times when prior terminus positions were known. Here, the calving rate, U_D, is defined as the difference between the average down-glacier ice velocity at the terminus and the change in terminus position in the x-direction over time:

$$U_D = \overline{U_T} - \frac{\partial x}{\partial t} \quad (8)$$

By treating calving in this manner, quantifying the rate of ice discharge over annual timescales requires only knowledge of yearly terminus position and an average ice velocity at the terminus. However, the controls on ice velocity are still poorly understood (e.g., Warren, 1999; Benn et al., 2007). To reduce unnecessary complexity, for this model run we ignore longitudinal stresses and assume resistance to flow is a product of lateral and basal drag.

Bathymetric transects along previous ice fronts, combined with an observed average height of the ice cliff above waterline of 40 m (H_o) allows us to determine the height of the ice front at the terminus (H_T), using a height above buoyancy criteria (Van der Veen, 1996), assuming the ice front is consistently close to flotation:

$$H_T = \frac{\rho_{sw}}{\rho_i} H_W + H_o \quad (9)$$

Water depth (H_w) hence is the primary control on terminus position and thinning will result in retreat until shallower water is reached. Once the ice height H_T and change in the glacier surface slope θ is known, the driving stress in the downslope direction can be quantified:

$$\tau_D = \rho_i g H_T \sin\theta \quad (10)$$

TCD
5, 1123–1166, 2011

This driving stress is opposed by basal resistance, which can be adjusted using a single tuning parameter C:

$$\tau_B = \tau_D \left(1 - \frac{\rho_w z}{\rho_i H_T}\right)^C \quad (11)$$

where $\rho_w z$ is the basal water pressure, and assuming that (a) $\tau_B = 0$ when the ice pressure $\rho_i H_T$ equals the basal water pressure, and (b) $\tau_B = \tau_D$ when $\rho_w z = 0$. C was tuned to calibrate the calving model to observed surface velocities in 1983, 1994, and 2001 (Naruse, 1985; Rignot et al., 1996; E. Rignot, personal communication, 2003); agreement was closest when $C = 0.6$. This is double the value of C calculated using data from Columbia Glacier (Benn et al., 2007), which could in due in part to Columbia Glacier's more gradual slope (1.15° versus 3.5° at Glaciar San Rafael) (Venteris, 1999).

The annual velocity at the terminus was then calculated assuming a rectangular bed and the sliding law developed by Benn et al. (2007). Mean values of basal drag, driving stress and ice height were used to estimatey the average sliding velocity U_B at the terminus:

$$U_B = \frac{2A}{n+1}\left(\frac{\tau_D - \tau_B}{H_T}\right)^n W^{n+1} \quad (12)$$

using a flow parameter A calculated from Arrhenius' Law and $n = 3$ from Glen's flow law (Nye, 1965). For our purposes, we assume a uniform vertical velocity distribution and consistent basal drag across the bed, allowing us to assume U_B equals the surface velocity (Howat et al., 2005). It follows that sliding velocity is most sensitive to changes in both ice thickness H_T relative to water depth and the glacier channel half-width W. Although this model does not take into account longitudinal stress gradients or water penetration in crevasses, it does manage to capture the approximate calving rate (see brown dots in Fig. 12, and Table 2).

The modeled annual velocities at the terminus, using $C = 0.6$ and the known terminus positions and water depths from Figs. 6 and 7, are listed in Table 2. The modeled velocities agree well with the observed surface velocities at the terminus from

TCD
5, 1123–1166, 2011

1983, 1994, and 2001. Terminus velocities were very large between 1959–1979 (6–9 km a^{-1}) when the glacier extended a considerable distance into Laguna San Rafael with much lower values of lateral drag. As the glacier receded to its present day position in the narrowing fjord, velocities decreased to ~3.3 km a^{-1}. Retreat rates are small (<200 m a^{-1}) compared with the large velocities modeled at the terminus of the glacier, thus calving rates were almost equal to down-glacier velocity (see Eq. 8). The resulting calving fluxes (the product of the calving rate U_D multiplied by the terminus cross-sectional area A_{term}) follow a similar trend to the results from the mass budget model in Sect. 5.4. However, the magnitude of the calving fluxes range from ~6 km^3 a^{-1} during 1960–1976, to 2.85 km^3 a^{-1} from 1977–1989, to 1.63 km^3 a^{-1} from 1990 (red dots in Fig. 12), exceeding those of the mass budget model (black line in Fig. 12) by 40% to 300%.

Results from the "sliding law" model in Table 2 indicates a relatively robust correlation ($r^2 = 0.76$) between the half width of the fjord channel and the modeled glacier velocity, suggesting that modeled ice velocities are controlled primarily by changes in the channel width, where wide channels allow for substantially lower values of lateral drag. By comparison, the sliding model also indicates a negligible dependence on water depths: modeled calving rates did not correlate with either mean water depth ($r^2 = 0.0008$) or maximum water depth ($r^2 = 0.014$).

Sensitivity analyses, carried out using the 2001 modeled calving rate for its relatively good fit with observations (E. Rignot, personal communication, 2003; Willis et al., 2010), suggest that the calving rate is particularly susceptible to changes in tuning parameter C, in Eq. (11). Peak calving rates occur when $C > 3$, where terminus velocities approach 16 km a^{-1} and any further increases in C have very little effect. Similarly, when C approaches 0, the calving rate also decreases rapidly, until it approaches zero. Raising the height above waterline (H_o), adding to the vertical ice face at the terminus, also decreases ice velocity. Although an increase in ice thickness should enhance the driving stress, it increases basal drag more substantially. While the driving stress is tempered by a low slope angle θ, the loading of ice onto the terminus will increase

TCD
5, 1123–1166, 2011

the downward pressure, increasing basal shear and lowering flow rates. Increasing the surface slope of the glacier, assuming there are no other changes to the system, results in a power law increase in terminus velocity and hence calving rate. Small increases in slope of the glacier result in significant increases in terminus velocity, allowing for rapid surges and appreciable increases in calving. This, however, assumes that the same thickness of ice, and therefore the same downward acting forces will drive glacier flow. In reality, we expect significant thinning associated with any increase in glacier slope, which has the potential to further enhance calving rates.

The modeled calving fluxes using Benn et al.'s "sliding laws", although greater than both observed and modeled mass balance fluxes, indicate a high degree of correlation between channel width, flow speed and calving rate. This behavior is key to understanding why most stable tidewater glaciers have termini located at topographic narrows, and why calving fluxes at Glaciar San Rafael decreased 2–5 fold, regardless of model scenario used, when the terminus retreated into the narrowing outlet east of the Andean range front. However, the difference in the magnitude of the calving fluxes between the sliding and balance flux models also suggests that calving dynamics may be more variable than the simple approximation of plug flow and lateral drag depicted in Eqs. (10)–(12).

Model limitations and sensitivities

Several studies have suggested that pronounced longitudinal stretching of glacier ice in the terminal zone may be a fundamental control on rapidly calving tidewater glaciers, promoting calving rates in excess of the balance flux of the glacier and resulting in retreat (e.g. Meier and Post, 1987; Venteris et al., 1997; Benn et al., 2007). If terminus retreat varies with increases in ice delivery to the terminus, as has been observed at other calving glaciers in the past decade (e.g. Howat et al., 2005; Luckman et al., 2006), retreat rates should increase in concert with increases in this calving flux. In contrast, our observations and model results from Glaciar San Rafael indicate that retreat rates increased during periods when the calving flux decreased in the early

TCD
5, 1123–1166, 2011

1980s and 1990s, while a short period of rapid retreat in the first few years of the 21st century appears to coincide with an increase in the calving flux. This relationship holds whether the calving flux is modeled using an ice mass budget (Sect. 5.4) or using terminus velocities and ice front bathymetry (Sect. 5.5)

At Glaciar San Rafael, retreat does not appear to co-vary with the calving flux, and in fact in fact is generally out of phase with Q_{calv}. This suggests that several of our inputs, assumptions and sensitivities may need revisiting. It is possible that the spatial distribution of accumulation in our model, which focuses the concentration of orographic precipitation around the ELA zone, is incorrect. In addition, caution is needed when assuming that surface lowering is driven exclusively by dynamic thinning. Nevertheless, our model results are consistent with observations across the region.

7 Implications for future behaviour

The geometry of Glaciar San Rafael, with a broad, relatively flat accumulation area and ELA zone funneled into a narrow constriction across the hanging wall of the Liquiñe-Ofqui fault and into Laguna San Rafael, renders the glacier capable of withstanding a substantially warmer and drier climate without necessarily resulting in retreat of the glacier snout. The rate of retreat is a function of competing influences between both climate and terminus geometry. For example, in 1986, when the terminus retreated across the rangefront and into the narrow valley constriction, the rate of retreat temporarily slowed, although calving speeds most probably did not. Moreover, although the terminus has not retreated substantially during the past few decades, the entire glacier has thinned significantly (Rivera et al., 2007) due to warming since the early 1980s.

Contrary to what has been observed at other tidewater glaciers, such as Marinelli Glacier (Koppes et al., 2009) or the outlet glaciers of Greenland (Thomas et al., 2003; Howat et al., 2005; Stearns and Hamilton, 2007), negative balance flux and accelerated surface thinning at Glaciar San Rafael over the past few decades has not (as of

TCD
5, 1123–1166, 2011

yet) resulted in a substantial increase in the rate of terminus retreat. However, considering that the ice thickness at the ELA is estimated to be only ~400 m (Rignot et al., 2003), continuous thinning rates of 1–2 m a^{-1} over the broad plateau of the icefield in the vicinity of the ELA would remove most of the glacier (and potentially most of the North Patagonian Icefield) within a few hundred years. Such substantial changes in the balance flux and the ice thickness would also affect buoyancy at the glacier terminus. Further, continuous rapid calving rates into water depths of ~210 m will likely destabilize the terminus and result in drastic retreat in the coming decades.

8 Conclusions

The annual budget of ice into and out of Glacier San Rafael over 1950–2005 was reconstructed using daily values of key climate variables from the NCEP-NCAR global reanalysis dataset and a compendium of historical observations. Using a DEM of the glacier surface and this reanalysis dataset, constrained by a sparse collection of direct measurements of local temperature, precipitation, ablation and thinning collected over the past few decades and a documented retreat of the terminus over the past ~50 yr, we estimated the annual accumulation, ablation and thinning fluxes over the glacier and the corresponding calving flux from the terminus during this time.

San Rafael glacier experienced a period of accelerated retreat starting around 1975 through the early 1990s, a period when accumulation decreased and ablation increased. Terminus retreat rates have been relatively low over the most recent decade, in part because the glacier is still experiencing rapid ice flow to the terminus and because it has retreated into a narrow outlet, limiting the contribution of ice-front melt to the overall mass loss. Our model results indicate that the decrease in net accumulation and increase in ablation over the last few decades, as the climate has become warmer and drier, has primarily resulted in pervasive thinning through both surface mass loss and accelerated flow. For Glaciar San Rafael, and possibly all glaciers of similar geometry with a broad plateau at the ELA and a narrow outlet, response to climate changes are reflected primarily in changes in the rate of surface thinning and

TCD
5, 1123–1166, 2011

the calving rate, and only secondarily in changes in terminus position, emphasizing the complex dynamics between climate inputs and glacier response.

Constrained by a few direct observations of Glaciar San Rafael's dynamics over the past few decades, we have calculated accumulation and ablation rates as a function of surface elevation to reconstruct the changing flux of ice to the terminus over the past ~50 yr. Comparison of results from our mass budget model with a reconstructed calving flux using theoretical calving and sliding laws, suggests that the trends in calving fluxes are robust, with calving rates decreasing during periods of rapid retreat in the late 1970s and 1980s; however, applying a "calving law" approach increases modeled calving rates by 40–300%. Our approach provides a simple reconstruction of the time-varying budget of ice through San Rafael glacier using sparse empirical data which, when compared with the history of the terminus retreat gleaned from maps, aerial photos and satellite images, together with topographic and bathymetric constraints of the proglacial lagoon into which it calves, illuminates the relative importance of climatic and non-climatic controls on the retreat of calving glaciers over annual to decadal time scales.

Acknowledgements. This work was supported by US NSF grant OPP-0338371 (Koppes), and NASA subcontract #1267029 through Eric Rignot at JPL (Conway and Rasmussen). We thank Bernard Hallet for stimulating discussions and support of this work. We also thank Gerard Roe for assistance with the orographic model, Andres Rivera for providing the Landsat imagery used in Fig. 1, Harvey Greenberg for assistance with the DEM construction, and Drew Stolar for assistance with GIS and MATLAB manipulation of the datasets.

References

Aniya, M.: Glacier inventory for the Northern Patagonia Icefield, Chile, and variations 1944/45 to 1985/86, Arctic Alpine Res., 20, 179–187, 1988.

Aniya, M.: Recent glacier variations of the Hielos Patagonicos, South America, and their contribution to sea-level change, Arct. Antarct. Alp. Res., 31(2), 165–17, 1999.

Araneda, A., Torrejón, F., Aguayo, M., Torres, L., Cruces, F., Cisternas, M., and Urrutia, R.:

TCD

5, 1123–1166, 2011

Historical records of San Rafael Glacier advances (North Patagonian Icefield): another clue to “Little Ice Age” timing in southern Chile?, Holocene, 17, 987–998, 2007.
Benn, D. I., Hulton, N. R. J., and Mottram, R. H.: Calving laws, “sliding laws” and the stability of tidewater glaciers, Ann. Glaciol., 46, 123–130, 2007.
Braithwaite, R. J. and Olesen, O. B.: Calculation of glacier ablation from air temperature, West Greenland, in: Glacier Fluctuations and Climatic Change, edited by: Oerlemans, J., Kluwer Academic, 219–233, 1989.
Carrasco, J., Casassa, G., and Rivera, A.: Meteorological and climatological aspects of the Southern Patagonia Icefield, in: The Patagonian ice fields: a unique natural laboratory for environmental and climate change studies, edited by: Casassa, G., Sepulveda, F. V., and Sinclair, R., New York, Kluwer Academic/Plenum Publishers, 29–41, 2002.
Cook, K. H., Yang, X., Carter, C. M., and Belcher, B. N.: A modeling system for studying climate controls on mountain glaciers with application to the Patagonian Icefields, Climate Change, 56, 339–367, 2003.
Enomoto, H. and Nakajima, C.: Recent climate-fluctuations in Patagonia, in: Glaciological Studies in Patagonia Northern Icefield 1983–1984, Nagoya (Japan), edited by: Nakajima, C, 7–14, 1985.
Escobar, F., Vidal, F., Garin, R., and Naruse, R.: Water balance in the Patagonain Icefield, in: Glaciological Researches in Patagonia, 1990, Nagoya (Japan), edited by: Naruse, R. and Aniya, M., 109–119, 1992.
Fujiyoshi, Y., Kondo, H., Inoue, J., and Yamada, T.: Characteristics of precipitation and vertical structure of air temperature in northern Patagonia, Bull. Glacier Res., 4, 15–24, 1987.
Howat, I. M., Joughin, I., Tulaczyk, S., and Gogineni, S.: Rapid retreat and acceleration of Helhiem Glacier, east Greenland, Geophy. Res. Lett., 32, L22502, doi:10.1029/2005GL024737, 2005.
Hubbard, A. L.: Modelling climate, topography and paleoglacier fluctuations in the Chilean Andes, Earth Surf. Proc. Land., 22, 79–92, 1997.
Hulton, N., Sugden, D., Payne, A., and Clapperton, C.: Glacier modeling and the climate of Patagonia during the Last Glacial Maximum, Quaternary Res., 42, 1–19, 1994.
Kalnay, E., Kanamitsu, M., Kistler, R., Collins, W., Deaven, D., Gandin, L., Iredell, M., Saha, S., White, G., Woollen, J., Zhu, Y., Chelliah, M., Ebisuzaki, W., Higgins, W., Janowiak, J., Mo, K. C., Ropelewski, C., Wang, J., Leetmaa, A., Reynolds, R., Jenne, R., and Joseph, D.: The NCEP/NCAR 40-year reanalysis project, B. Am. Meteorol. Soc., 77, 437–471, 1996.

TCD
5, 1123–1166, 2011

Kistler, R., Kalnay, E., Collins, W., Saha, S., White, G., Woollen, J., Chelliah, M., Ebisuzaki, W., Kanamitsu, M., Kousky, V., van de Dool, H., Jenne, R., and Fiorino, M.: The NCEP-NCAR 40-year reanalysis: monthly means CD-ROM and documentation, B. Am. Meteorol. Soc., 82, 247–267, 2001.

Kobayashi, S. and Saito, T.: Meteorological observations on Soler Glacier, in: Glaciological Studies in Patagonia Northern Icefield 1983–1984, Nagoya (Japan), edited by: Nakajima, C., 32–36, 1985.

Kondo, H. and Yamada, T.: Some remarks on the mass balance of the terminal-lateral fluctuations of San Rafael Glacier, the Northern Patagonia Icefield, Bull. Glacier Res., 6, 55–63, 1988.

Koppes, M., Hallet, B., and Anderson, J.: Synchronous acceleration of ice loss and glacier erosion, Marinelli Glacier, Tierra del Fuego, J. Glaciol., 55, 207–220, 2009.

Koppes, M., Sylwester, R., Rivera, A., and Hallet, B.: Sediment yields over an advance-retreat cycle of a calving glacier, Laguna San Rafael, North Patagonian Icefield, Quaternary Res., 73, 84–95, 2010.

Koppes, M. N.: Glacier erosion and response to climate, from Alaska to Patagonia, Ph.D. thesis, University of Washington, USA, 228 pp., 2007.

Lamy, F. J., Kaiser, J., Ninnemann, U., Hebbeln, D., Arz, H. W., and Stoner, J.: Antarctic timing of surface water changes off Chile and Patagonian ice sheet response, Science, 304, 959–1962, 2004.

Luckman, A., Murray, T., de Lange, R., and Hanna, E.: Rapid and synchronous ice-dynamic changes in East Greenland, Geophys. Res. Lett., 33, L03503, doi:10.1029/2005GL025428, 2006.

Matsuoka, K. and Naruse, R.: Mass balance features derived from a firn core at Hielo Patagonico Norte, South America, Arct. Antarct. Alp. Res., 31, 333–340, 1999.

Mayr, C., Wille, M., Haberzetti, T., Fey, M., Janssen, S., Lucke, H., Ohlendorf, C., Oliva, G., Schabitz, F., Schleser, G. H., and Zolitschka, B.: Holocene variability of the Southern Hemisphere westerlies in Argentinean Patagonia (52° S), Quaternary Sci. Rev., 26(5–6), 579–584, 2007.

Meier, M. F. and Post, A.: Fast tidewater glaciers, J. Geophys. Res., 92(B9), 9051–9058, 1987.

Motyka, R. J., Hunter, L., Echelmeyer, K. A., and Connor, C.: Submarine melting at the terminus of a temperate tidewater glacier, LeConte Glacier, Alaska, U.S.A., Ann. Glaciol., 36, 57–65, 2003.

TCD
5, 1123–1166, 2011

Naruse, R.: Flow of Soler Glacier and San Rafael Glacier, in: Glaciological Studies in Patagonia Northern Icefield 1983-1984, Nagoya (Japan), edited by: Nakajima, C., 32–36, 1985.
Nye, J. F.: The flow of a glacier in a channel of rectangular elliptic and parabolic cross-section, J. Glaciol., 5(41), 661–690, 1965.
Ohata, T., Enomoto, H., and Kondo, H.: Characteristic of ablation at San Rafael Glacier, in: Glaciological Studies in Patagonia Northern Icefield 1983–1984, Nagoya (Japan), edited by: Nakajima, C., 37–45, 1985a.
Ohata, T., Kondo, H., and Enomoto, H.: Meteorological observations at San Rafael Glacier, in: Glaciological Studies in Patagonia Northern Icefield 1983–1984, Nagoya (Japan), edited by: Nakajima, C., 22–31, 1985b.
O'Neel, S., Pfeffer, W. T., Krimmel, R., and Meier, M.: Evolving force balance and Columbia Glacier, Alaska, during rapid retreat, J. Geophys. Res., 110, F03012, doi:10.1029/2005JF000292, 2005.
Pfeffer, W. T.: A simple mechanism for irreversible tidewater glacier retreat, J. Geophys. Res., 112, F03S25, doi:10.1029/2006JF000590, 2007.
Powell, R. D.: Grounding-line systems as second-order controls on fluctuations of tidewater termini of temperate glaciers, in: Glacial marine sedimentation; Paleoclimatic significance, Geological Society of America Special Paper 261, edited by: Anderson, J. B. and Ashley, G. M., 75–94, 1991.
Rasmussen, L. A. and Conway, H.: Estimating South Cascade Glacier (Washington, U.S.A.) mass balance from a distance radiosonde and comparison with Blue Glacier, J. Glaciol., 47(159), 579–588, 2001.
Rasmussen, L. A., Conway, H., and Raymond, C. F.: Influence of upper-air conditions on the Patagonia icefields, Global Planet. Change, 59, 203–216, 2007.
Rignot, E., Forster, R., and Isacks, B.: Interferometric radar observations of Glaciar San Rafael, Chile, J. Glaciol., 42(141), 279–291, 1996.
Rignot, E., Rivera, A., and Casassa, G.: Contribution of the Patagonia Icefields of South America to sea level rise, Science, 302, 434–437, 2003.
Rignot, E., Koppes, M., and Velicogna, I.: Rapid submarine melting of the calving faces of west Greenland glaciers, Nat. Geosci., 3, 187–191, 2010.
Rivera, A., Benham, T., Casassa, G., Bamber, J., and Dowdeswell, J.: Ice elevation and areal changes of glaciers from the North Patagonia Icefield, Chile, Global Planet. Change, 59, 126–137, doi:10.1016/j.gloplacha.2006.11.037, 2007.

TCD
5, 1123–1166, 2011

Roe, G. H.: Orographic precipitation, Annu. Rev. Earth Pl. Sc., 33, 645–671, 2005.
Smith, R. B. and Barstad, I.: A linear theory of orographic precipitation, J. Atmos. Sci., 61, 1377–1391, 2004.
Stearns, L. A. and Hamilton, G. S.: Rapid volume loss from two East Greenland outlet glaciers quantified using repeat stereo satellite imagery, Geophys. Res. Lett., 34, L05503, doi:10.1029/2006GL028982, 2007.
Thomas, R. H., Abdalati, W., Frederick, E., Krabill, W. B., Manizade, S., and Steffen, K.: Investigation of surface melting and dynamic thinning on Jakobshavn Isbrae, Greenland, J. Glaciol., 49, 231–239, 2003.
Van der Veen, C.: Tidewater calving, J. Glaciol., 42, 375–385, 1996.
Venteris, E. R.: Rapid tidewater glacier retreat: a comparison between Columbia Glacier, Alaska and Patagonian calving glaciers, Global Planet. Change, 22, 131–138, 1999.
Venteris, E. R., Whillans, I. M., and Van der Veen, C. J.: Effect of extension rate on terminus positions, Columbia Glacier, Alaska, USA, Ann. Glaciol., 24, 49–53, 1997.
Warren, C. R.: Rapid recent fluctuations of the calving San Rafael Glacier, Chilean Patagonia: climatic or non-climatic?, Geogr. Ann. A, 75, 111–125, 1993.
Warren, C. R. and Aniya, M.: The calving glaciers of southern South America, Global Planet. Change, 22, 59–77, 1999.
Warren, C. R. and Sugden, D. E.: The Patagonian Icefields: a glaciological review, Arctic Alpine Res., 25(4), 316–331, 1993.
Warren, C. R., Glasser, N. F., Harrison, S., Winchester, V., Kerr, A., and Rivera, A.: Characteristics of tide-water calving at Glaciar San Rafael, Chile, J. Glaciol., 41(138), 273–289, 1995.
Willis, M. J., Melkonian, A. K., Pritchard, M. E., and Bernstein, S.: Remote sensing of velocities and elevation changes at outlet glaciers of the Northern Patagonian Icefield, Chile, International Glaciological Conference Ice and Climate Change: A View from the South, Valdavia, Chile, February 2010.
Wratt, D. S., Revell, M. J., Sinclair, M. R., Gray, W. R., Henderson, R. D., and Chater, A. M.: Relation between are mass properties and mesoscale rainfall in New Zealand's Southern Alps, Atmos. Res., 52, 261–282, 2000.
Yamada, T.: Glaciological characteristics revealed by 37.6 m deep core drilled at the accumulation area of San Rafael Glacier, the Northern Patagonia Icefield, Bull. Glacier Res., 4, 59–67, 1987.

TCD
5, 1123–1166, 2011

Table 1. Summary of modeled ice fluxes through Glaciar San Rafael, 1960–2005.

Cases[1]	Q_{abl} average 1960–2005 $km^3\ a^{-1}$	Q_{acc} average 1960–2005 $km^3\ a^{-1}$	Q_{bal} 1960–1976 $km^3\ a^{-1}$	Q_{bal} 1977–1989 $km^3\ a^{-1}$	Q_{bal} 1990–2005 $km^3\ a^{-1}$	Q^2_{calv} 1960–1976 $km^3\ a^{-1}$	Q^2_{calv} 1977–1989 $km^3\ a^{-1}$	Q^2_{calv} 1990–2005 $km^3\ a^{-1}$
#1: $\alpha 1$, $k=3$	4.40	3.91	0.1	−1.38	−0.38	0.53	−0.79	0.01
#2: $\alpha 2$, $k=3$	4.20	3.91	0.29	−1.19	−0.11	0.72	−0.61	0.18
#3: $\alpha 2$, $k=5$	4.20	6.52	3.21	1.07	2.46	3.68	1.74	2.75
#4: $\alpha 2$, $k(z)$	4.20	4.97	1.45	−0.25	0.91	1.89	0.37	1.21
		Q_{thin}	0.32	0.75	0.43			
		Q_{term}	0.05	0.09	0.04			

[1] Scenarios used in model runs: $\alpha 1$ = ablation flux using Eq. (4a) only; $\alpha 2$ = ablation flux calculated using Eq. (4a) and (4b); $k(z)$ = enhancement factor used in Eq. (3).

[2] Q_{calv} is calculated as in Eq. (7) as the sum of Q_{thin}, Q_{bal} and Q_{term}. Q_{thin} and Q_{term} did not vary from case to case.

TCD
5, 1123–1166, 2011

Table 2. Modeled velocities at the terminus using "sliding laws" developed in Benn et al. (2007), for years with known terminus positions and bathymetric data, and observed terminus velocities for years with available data (Kondo and Yamada, 1988; Warren et al., 1995; Rignot et al., 1996; Willis et al., 2010). Calving rates calculated according to definition in Eq. (8). Calving fluxes calculated as product of calving rate and ice front area.

Year	Velocity ($km\,a^{-1}$)	Observed Velocity ($km\,a^{-1}$)	Terminus width (m)	Ice front halfwidth W (m)	Max water depth (m)	Mean water depth (m)	Retreat rate ($m\,a^{-1}$)	Calving rate ($km\,a^{-1}$)	Calving flux ($km^3\,a^{-1}$)
2001	3.40	3.08	2160	1053	254	164	80	3.33	1.49
1998	3.25		2400	1117	267	152	50	3.20	1.5
1994	3.32	4–6	2280	1117	249	141	69	3.25	1.79
1992	3.51		2800	1117	27	166	133	3.37	1.75
1989	4.72		2500	1170	281	177	201	4.52	2.49
1986	5.01		2760	1383	265	177	12	5.00	2.75
1983	6.17	5.11	2310	1319	217	139	96	6.07	3.34
1979	9.33		3750	1372	276	180	170	9.16	7.33
1976	7.91		4550	1362	237	157	139	7.77	6.68
1965	6.01		4870	1362	205	129	47	5.97	5.37
1959	8.95		5350	1489	259	131	5	8.94	8.05

TCD
5, 1123–1166, 2011

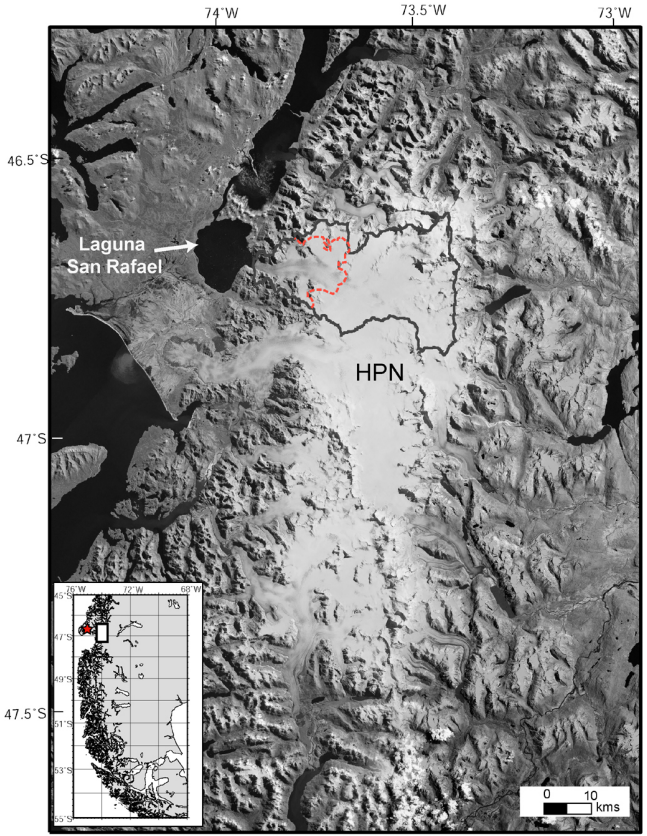

Fig. 1. Location of Glaciar San Rafael in the Campo de Hielo Patagonico Norte (HPN), Chile. Solid-line marks map extent of the glacier; dashed-line indicates present-day equilibrium line (about 1200 m a.s.l.). The glacier calves into Laguna San Rafael (LSR). The star shown in the inset map is the location of the NCEP-NCAR grid point SR1.

TCD
5, 1123–1166, 2011

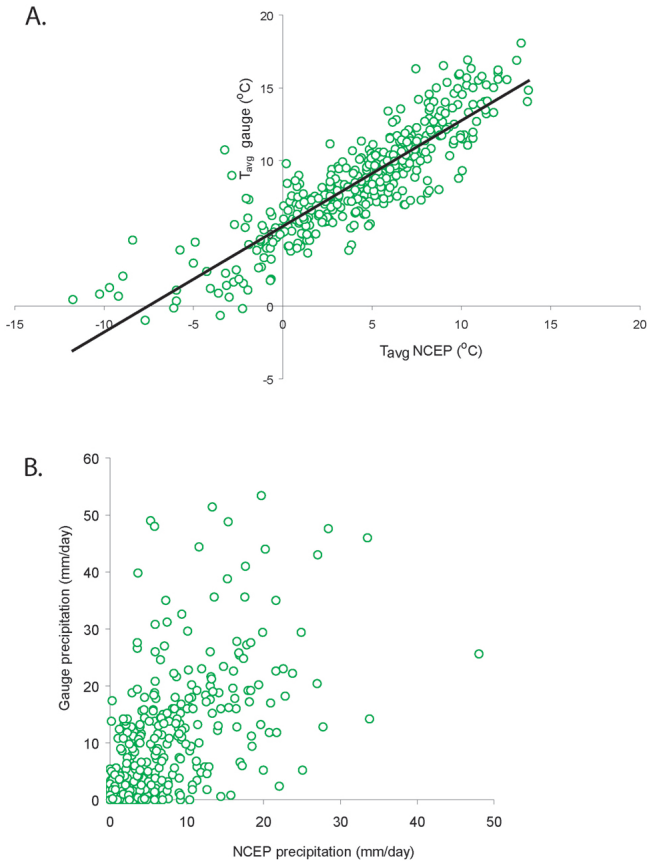

Fig. 2. Comparison of daily-average measurements of temperature **(A)** and precipitation **(B)** made at Laguna San Rafael from March 2005 to April 2006, with NCEP-NCAR derived values at 2 m above ground at SR1.

TCD
5, 1123–1166, 2011

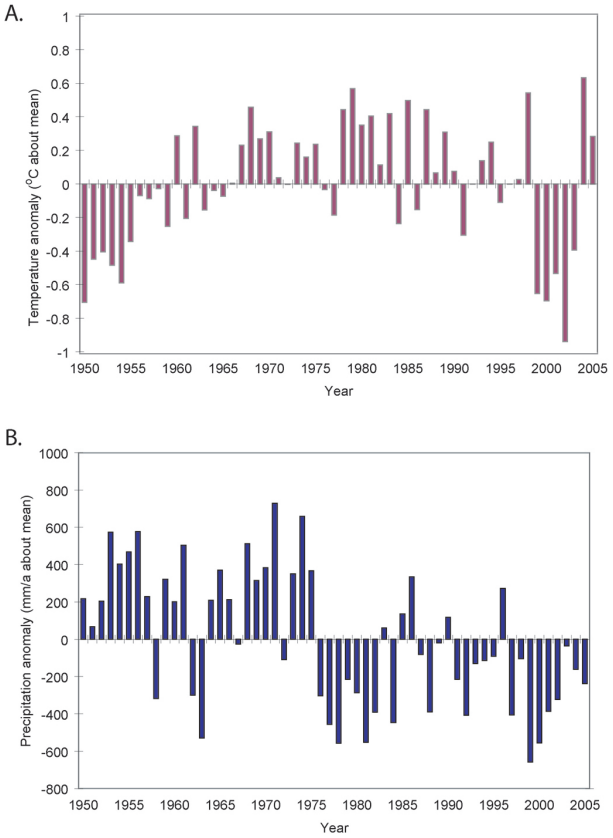

Fig. 3. Reconstructed annual temperature **(A)** and precipitation **(B)** anomalies at Laguna San Rafael for the period 1950 to 2005. Local values were calculated using NCEP-NCAR data and the relationships established in Eqs. (1) and (2). Anomalies shown are differences from the mean value for the period: mean annual temperature was 8.9 °C; mean annual precipitation at LSR was 3.60 m water equivalent.

TCD
5, 1123–1166, 2011

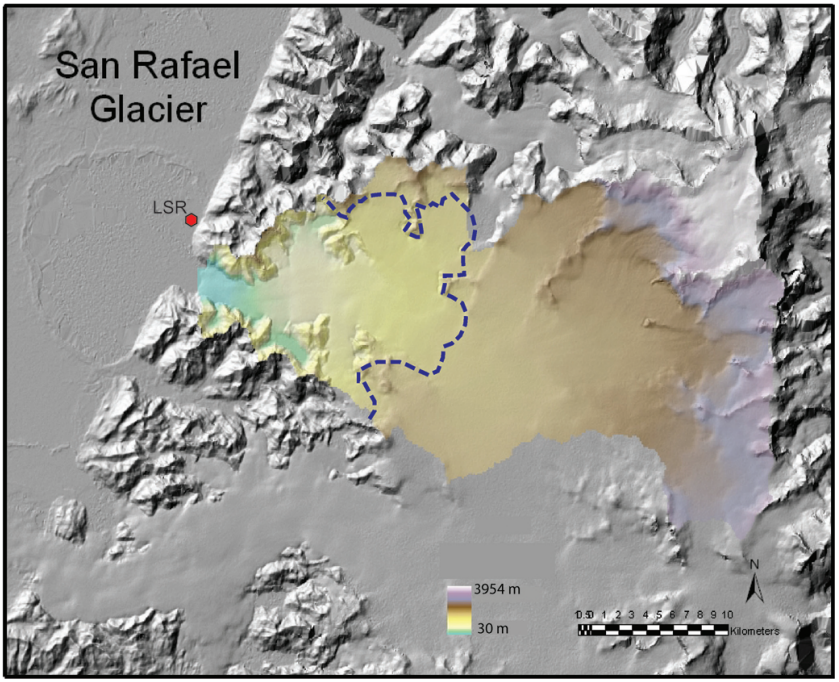

Fig. 4. Digital elevation model of Glaciar San Rafael obtained from SRTM-2000 data. Dashed blue line represents the mean ELA. Measurements of daily temperature and precipitation were collected at LSR along the rangefront.

TCD
5, 1123–1166, 2011

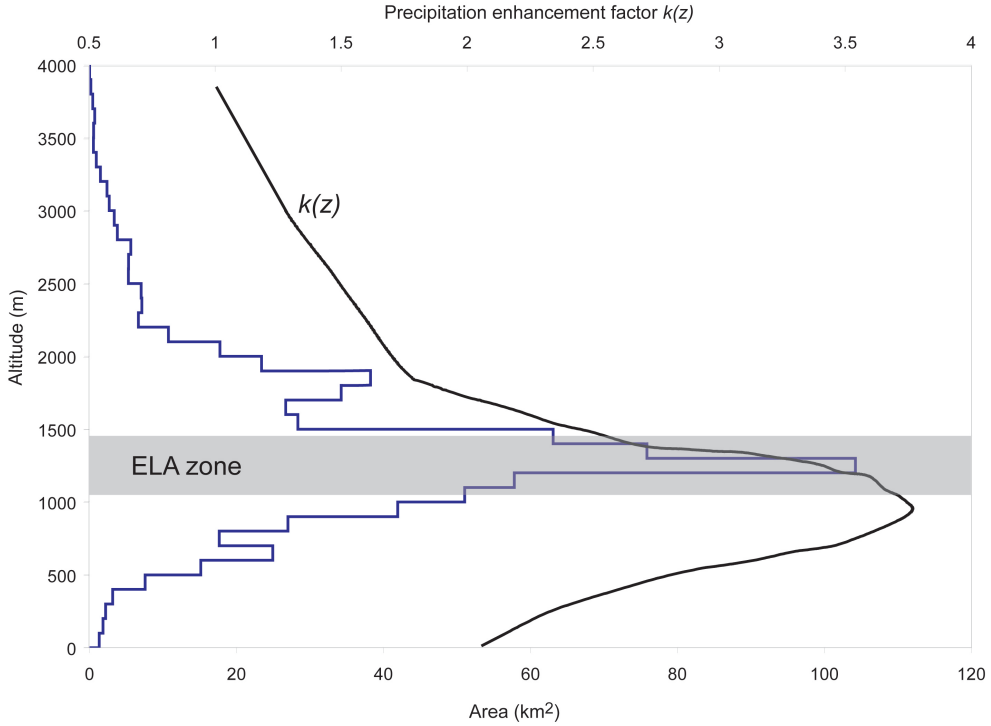

Fig. 5. Present-day area-altitude distribution of Glaciar San Rafael, in 100-m. altitude intervals, derived from SRTM-2000 data, and spatial variation in the precipitation enhancement factor $k(z)$ (black line) used to model precipitation on the glacier surface. The zone of equilibrium line altitudes from 1960–2005 is indicated by the grey bar.

TCD
5, 1123–1166, 2011

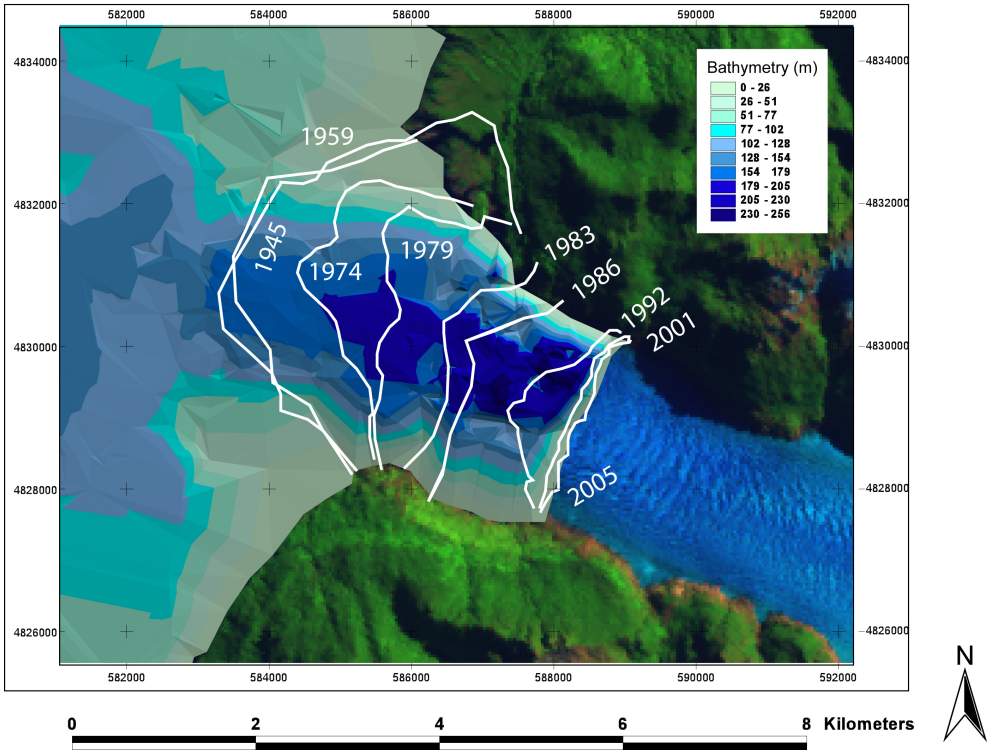

Fig. 6. Terminus positions of Glaciar San Rafael from 1945 to 2006, and bathymetry of Laguna San Rafael. The terminus was relatively stationary between 1945 and 1959, and again between 2001 and 2006. Bathymetry was mapped using ship-board sonar in 2005 and 2006.

TCD
5, 1123–1166, 2011

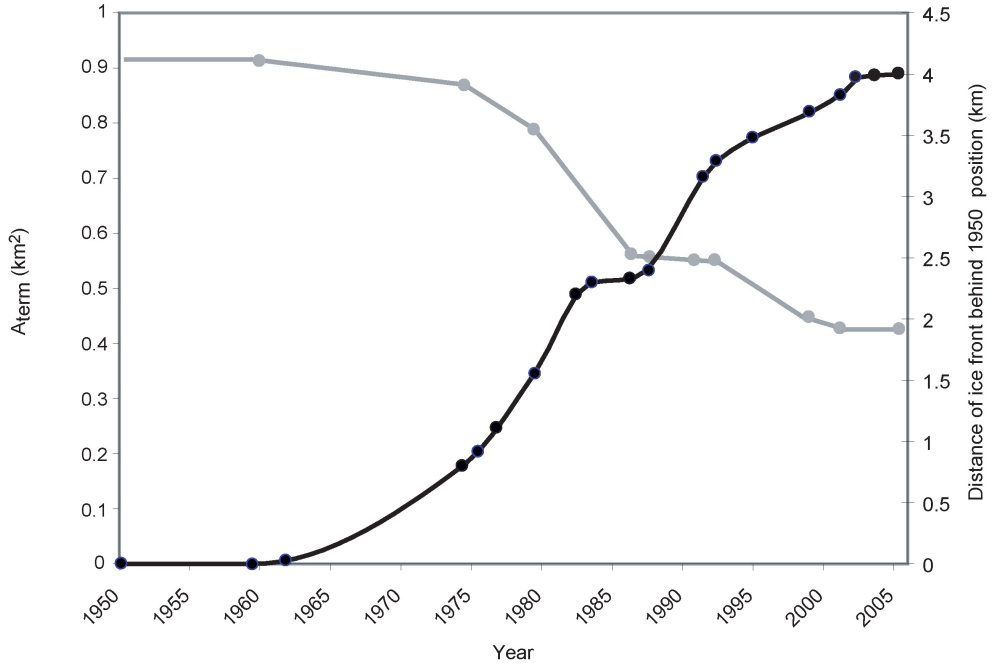

Fig. 7. History of the ice-front area A_{term} (grey line) calculated from the bathymetry of Laguna San Rafael, known terminus positions (black dots), and interpolated terminus positions (black line) (see Fig. 6). For the calculation of changes in A_{term} over time we assume that, on average, the cliff height across the terminus was 40 m above the water line.

TCD
5, 1123–1166, 2011

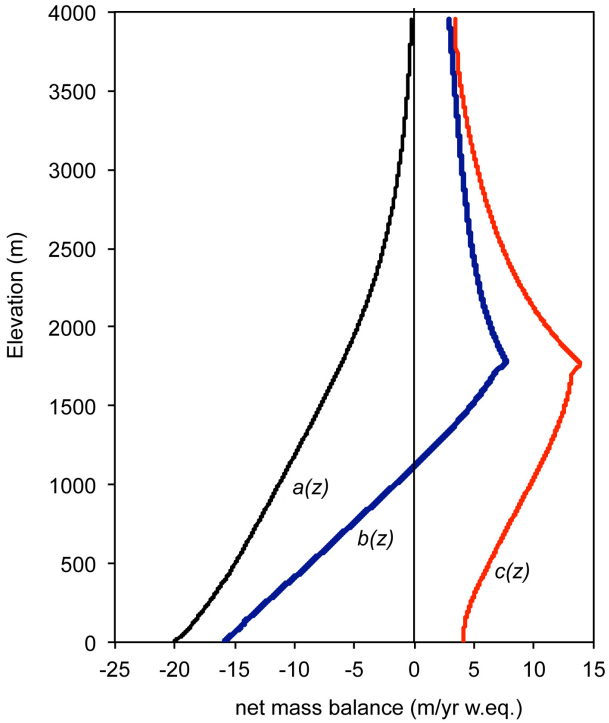

Fig. 8. Mean annual surface mass balance $b(z)$ derived from the mass balance model for the period 1960–2005, versus elevation.

TCD
5, 1123–1166, 2011

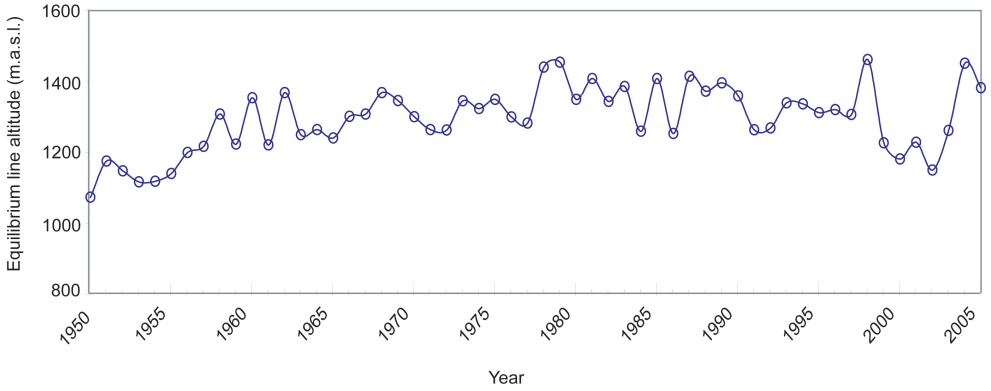

Fig. 9. Annual equilibrium line altitude (ELA) derived from the mass balance model, from 1950–2005.

TCD
5, 1123–1166, 2011

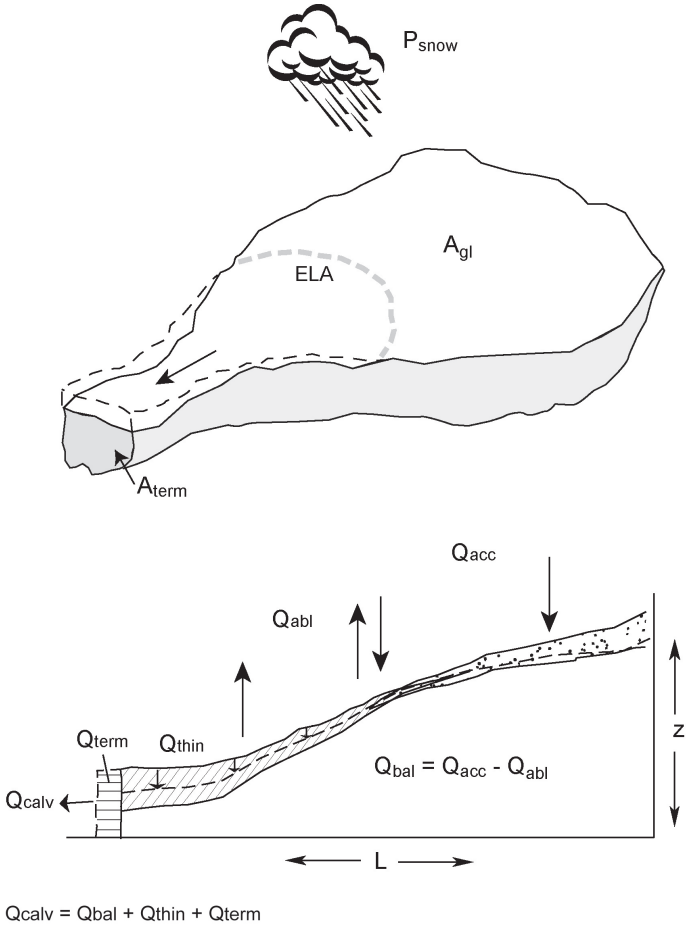

Fig. 10. Illustration of fluxes and areas relevant for estimating the mass budget of calving glaciers.

TCD
5, 1123–1166, 2011

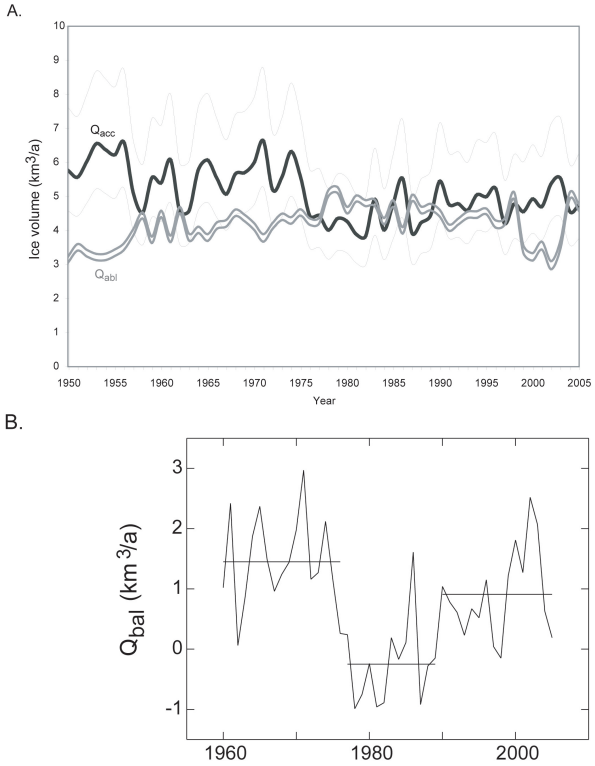

Fig. 11. Histories of **(A)** annual accumulation (black lines) and ablation (grey lines) from 1950–2005, and **(B)** surface mass balance Q_{bal} from 1960–2005. The range of accumulation fluxes Q_{acc}, derived from the various input cases listed in Table 1, are represented by the thin black lines in **(A)**. The two grey lines in **(A)** represent the upper and lower ranges of Q_{abl} derived from use of the two ablation co-efficients $\alpha 1$ (Eq. 4a) and $\alpha 2$ (Eq. 4a and 4b). The resulting surface mass balance flux shown in **(B)** is derived from input scenario #4 (Table 1). A piecewise linear fit was chosen to indicate averages over the periods 1960–1976, 1977–1989 and 1990–2005, as in Table 1 (dashed lines).

TCD
5, 1123–1166, 2011

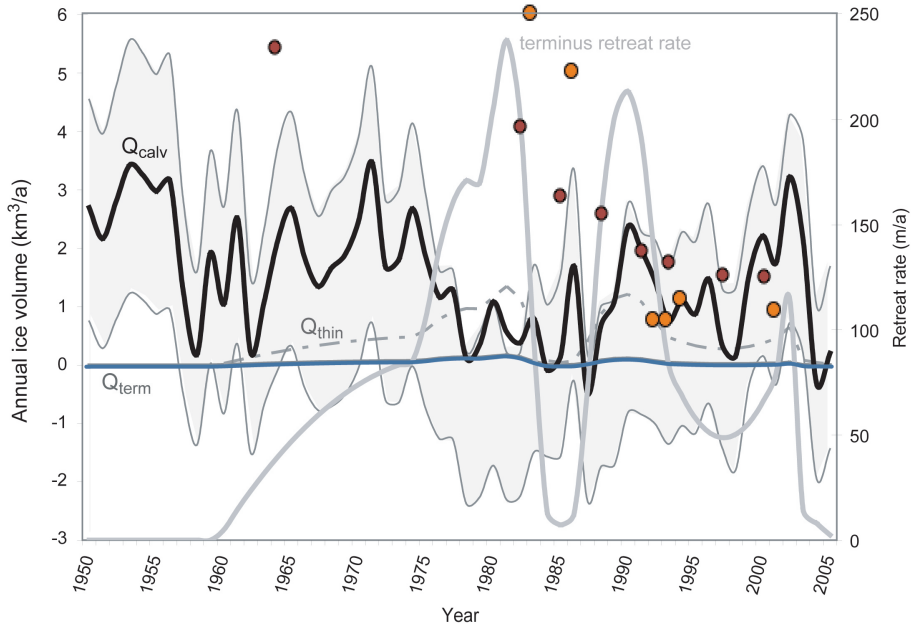

Fig. 12. Histories of surface thinning Q_{thin} (grey dashed line) ice loss from the terminus Q_{term} (blue line), calving flux Q_{calv} (black line and grey shading), and terminus retreat rate (grey line) from 1950–2005. The annual retreat rate is the derivative of the cubic spline fit to the points show in Fig. 7. The calving flux Q_{calv} was derived using the various input cases listed in Table 1: the black line represents the calving flux calculated using by the surface mass balance is derived from input scenario #4 (Fig. 11b), the grey shading indicates the range of derived calving fluxes from the various mass balance scenarios. The orange dots represent actual observed calving fluxes used to tune the models; the brown dots represent calving fluxes modeled using a "sliding law", listed in Table 2.

TCD
5, 1123–1166, 2011